Progress In Electromagnetics Research C, Vol. 110, 67–80, 2021

Dual Coaxial Probes in Transmission, Inserted by Dielectric with Two Different Thicknesses to Extract the Material Complex Relative Permittivity: Discontinuity Impacts

Franck Moukanda Mbango[1, *], Fabien Ndagijimana[2], and Aubin L. L. Okana[3]

Abstract—After a thorough investigation, this paper introduces a novel and simple radiofrequency material characterization technique. For this study's purposes, two probes were developed and separated by the sample under test (SUT) with an inhomogeneous test cell. Furthermore, the discontinuity impacts at the probe, SUT interfaces, were also studied. The investigation uses the transmission process through the principle of two different SUT thicknesses to measure its relative permittivity and loss tangent. The technique is based on using the lumped elements of an equivalent circuit of the entire test cell and covers 1 MHz–2 GHz. With the SUT, placed between two metal probes and another metallization, placed under its thickness on an opposite side to improve the loss tangent acquisition level, the cascading chain matrix (CCM) is used to get the final parameters. The thickness changing makes it possible to overcome the contact interface effects probe-sample. A mathematical model has also been presented through the fitting procedure. The new technique has been validated with three materials: Rogers RO4003C, FR-4 HTG-175, and Alumina 99.6%. The SUT complex relative permittivity extraction makes the new approach suitable for the telecommunication industry and many others. The method is also ideal for materials with thickness sizing up to 3 mm around.

1. INTRODUCTION

Material characterization has a wide variety of characterization techniques depending on the application domain [1], increasing the different degrees of understanding [2, 3]. Other material techniques are investigated in several laboratories to better understand the different material properties and behaviors [2, 4, 5]. From microwave theory, material characterization methods can be categorized into two forms: non-resonant [6] and resonant processes [7], which can also be subdivided into two techniques, namely through one port technique [8] and two ports technique [9–11]. Among several existing methods [12, 13], the probe or applicator method is well known [14–16]. It is either used for magnetic [17] or dielectric [18] materials.

In this paper, the electric field applicator (two circular coaxial probes) is applied to the solid or non-rigid materials, placed in a transmission system. The samples have to be shaped appropriately and subsequently de-embedded from the global measured S-parameters. The contact interface probe-sample presents some discontinuities on both sides, which can be extracted from the cascading chain matrix (CCM). The scattering parameters are measured over various frequency bands by using a vectorial network analyzer (VNA). The desired material parameters might be extracted numerically by equating the analytical results to each frequency's experimental measurements. During the method

Received 4 January 2021, Accepted 10 February 2021, Scheduled 19 February 2021

* Corresponding author: Franck Moukanda Mbango (franck.moukandambango@umng.cg).

[1] School of Sciences and Techniques, Electrical and Electronics Engineering Laboratory, Marien Ngouabi University, B. P 69, Brazzaville, Congo. [2] Electrical Engineering Department, Univ. Grenoble Alpes, CNRS, G2ELab, 151 Rue de la Papeterie, F-38400 St-Martin d'Hères, France. [3] School of Sciences and Techniques, Groupe de Simulations Numériques en Magnétisme et Catalyse, Université Marien Ngouabi, B. P 69, Brazzaville, Congo.

process development, it appears that the discontinuities' admittances and the transfer impedance can be removed. The transfer impedance gives crucial information on the insulator's state, as presented in the literature [11, 19–21]. The principle of concentrated elements, applied with two different thicknesses of identical material, is a new approach to characterize materials. Two methods are developed and presented in this paper: using discontinuities as a problem (sorting them out) or a solution (keep them in the process). Using the distributed element (transmission-line) methods, the discontinuities are parameters to solve [3, 22, 23]. The equations are inserted through algorithms as in many techniques [24] to extract the dielectric parameters. The test cell configuration and modeling are presented before the approach developments and experimental results to validate the new design and process in the wide frequency range of 1 MHz–2 GHz, where the specimen's fixture is inhomogeneous.

2. TEST CELL CONFIGURATION

The specimen test design is made with two circular coaxial probes. These probes are intercalated by the sample under test (SUT), as shown in Figure 1(a). The equivalent electric circuit of the global test cell is presented in Figure 1(b). l, h, and X are respectively the connector's length, SUT thickness (also endorsed as DUT for the device under test) and SUT length.

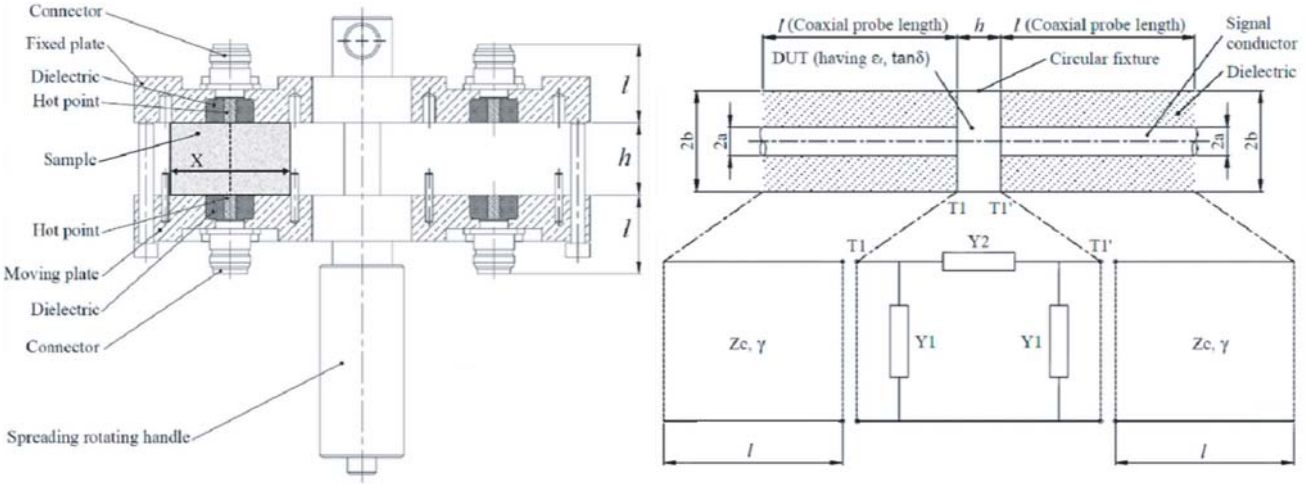

(a) (b)

Figure 1. (a) Slice view of the test cell. (b) Equivalent transmission line circuit of the test cell.

The material thickness is controlled when the system is tightened with the spreading rotating handle. However, we have to use a caliper to measure the numerical value of material thickness. The cell has two sides, where the feedlines (connector) are placed. One side is fixed when the second side is a moving plate to control the SUT thickness.

Figure 2 represents the approach of the simplified method using discontinuities or not. The two material thicknesses are represented by h_1 and h_2. Z_c and γ are respectively the characteristic impedance and propagation constant of the connectors that work as distributed elements while the SUTs behave as lumped elements.

3. EXTRACTION METHODS

Two approaches are developed to compare the impacts of discontinuities when using them or not. Unlike the two-line technique that uses the cascading wave matrix (CWM) through the mix of several transfer matrices [8, 25], we have applied the chain matrix combination to get the effective permittivity parameters. Firstly, all parts of the test fixture design are defined before developing each solution

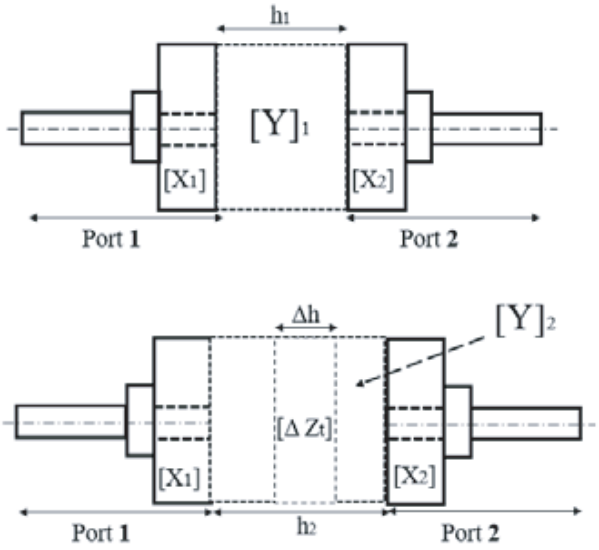

Figure 2. Procedure diagram of the method.

approach. So, for port 1 (connector) which is of length l

$$[X_1] = \begin{bmatrix} \cosh(\gamma_1 l) & Z_c^{(1)} \sinh(\gamma_1 l) \\ \dfrac{\sinh(\gamma_1 l)}{Z_c^{(1)}} & \cosh(\gamma_1 l) \end{bmatrix} \tag{1}$$

If we consider the minor mechanical differences, coming probably from the feedline dimensions during its designing stage, in that case,

$$[X_2] = \begin{bmatrix} \cosh(\gamma_2 l) & Z_c^{(2)} \sinh(\gamma_2 l) \\ \dfrac{\sinh(\gamma_2 l)}{Z_c^{(2)}} & \cosh(\gamma_2 l) \end{bmatrix} \tag{2}$$

As shown in Figure 1(a), the material thickness h changes according to the specimen and the approach to use. From Figure 1(b), when the SUT has a thickness of h_1, its chain matrix is given as follows:

$$[Y]_1 = \begin{bmatrix} 1 + \dfrac{Y_1}{Y_t^{(1)}} & \dfrac{1}{Y_t^{(1)}} \\ \dfrac{Y_1^2 + 2Y_1 Y_t^{(1)}}{Y_t^{(1)}} & 1 + \dfrac{Y_1}{Y_t^{(1)}} \end{bmatrix} \tag{3}$$

Also, for the thickness h_2, the chain matrix is written as below,

$$[Y]_2 = \begin{bmatrix} 1 + \dfrac{Y_1}{Y_t^{(2)}} & \dfrac{1}{Y_t^{(2)}} \\ \dfrac{Y_1^2 + 2Y_1 Y_t^{(2)}}{Y_t^{(1)}} & 1 + \dfrac{Y_1}{Y_t^{(2)}} \end{bmatrix} \tag{4}$$

The discontinuity at the contact interface probe — the material is represented by the admittance $Y_1 = -Y_d$. For the transfer impedance in each configuration, we have:

$$Z_t^{(1)} = \frac{1}{Y_t^{(1)}} \tag{5}$$

and,

$$Z_t^{(2)} = \frac{1}{Y_t^{(2)}} \tag{6}$$

When the thickness changes, it means that the condensators get modifications as well. The cascading chain matrix in each design is expressed as,

$$[M_1] = [X_1]\,[Y]_1\,[X_2] \tag{7}$$

$$[M_2] = [X_1]\,[Y]_2\,[X_2] \tag{8}$$

3.1. Method without Discontinuities at the Contact Interfaces

To reduce constraints, we assume that the two ports are electrically and mechanically identical. In that case, the cascading configuration can be expressed as follows:

$$[M_{12}] = [M_2]\,[M_1]^{-1} \tag{9}$$

$$[Y_{12}] = [Y]_2\,[Y]_1^{-1} = [\Delta Z_t]^{-1} \tag{10}$$

It is found that

$$[Y_{12}] = [X_1]^{-1}\,[M_{12}]\,[X_1] \tag{11}$$

At the same time, $[Y_{12}]$ can be written as follows

$$[Y_{12}] = \begin{bmatrix} A_{00} & B_{00} \\ C_{00} & D_{00} \end{bmatrix} \tag{12}$$

The resolution of Equations (9), (11), and (12) leads toward,

$$B_{00} = \frac{1}{Y_t^{(2)}} - \frac{1}{Y_t^{(1)}} = Z_t^{(2)} - Z_t^{(1)} \tag{13}$$

$$\Delta Z_t = Z_t^{(2)} - Z_t^{(1)} \tag{14}$$

In addition, the admittance existing at the contact interface appears as,

$$Y_d = -\frac{1 - A_{00}}{B_{00}} \tag{15}$$

We denote S the inner conductor's surface area (pointed out as a hot point in Figure 1(a)). The system is assumed to be a planar capacitor which can be mathematically modelized as given below:

$$Z_t^{(1)} = \frac{1}{j\omega\varepsilon_0\varepsilon^*_{eff}\dfrac{S}{h_1}} \tag{16}$$

$$Z_t^{(2)} = \frac{1}{j\omega\varepsilon_0\varepsilon^*_{eff}\dfrac{S}{h_2}} \tag{17}$$

When the material thickness changes from h_1 to h_2, it represents an increase of Δh such as,

$$\Delta h_{SUT}\,(mm) = h_2 - h_1 \tag{18}$$

And the transfer impedance without the impedances of discontinuities is computed from Equation (14) as follows:

$$\Delta Z_t = \frac{1}{j\omega\varepsilon_0\varepsilon^*_{eff}\dfrac{S}{h_2 - h_1}} = \frac{1}{j\omega\Delta C} \tag{19}$$

where S is the area of the central conductor of the probes. We note by ΔZ_t^v and ΔZ_t^m the structure impedance without discontinuities in the situation of vacuum and SUT respectively. If we associate Equations (13) and (19), the model used to get to the complex effective permittivity is defined as:

$$\varepsilon^*_{eff} = \frac{Z_t^v}{Z_t^m} = \frac{B_{00}^v}{B_{00}^m} \tag{20}$$

We name D as the outer diameter of the inner conductor of the circular coaxial probe. We have modeled the change from Equation (20) to the relative permittivity through a mathematic formulation as given below,

$$\varepsilon_r^* = \left(1 + \frac{\pi}{2}\frac{\Delta h_{SUT}}{D}\right)\varepsilon_{eff}^* \tag{21}$$

and

$$\varepsilon_r^* = \varepsilon_r' - j\varepsilon_r'' \tag{22}$$

The dielectric loss tangent is deducted from Equation (22) as given below,

$$\tan\delta = \frac{\varepsilon_r''}{\varepsilon_r'} \tag{23}$$

3.2. The Method with Discontinuities at the Contact Interfaces

The new approach consists of working with the impedances of discontinuities. The system is inhomogeneous, and the conductors' impacts are neglected. The equivalent circuit without probes is now an admittance of transfer, and Equations (7), (8) become,

$$[M_1]_N = [X_1]\left[Y_{tN}^{(1)}\right][X_2] \tag{24}$$

$$[M_2]_N = [X_1]\left[Y_{tN}^{(2)}\right][X_2] \tag{25}$$

The new concept is pointed out by the subscript "N", which is the probes' test cell approach, operating in transmission. From these two last equations, the admittance of transfer might be determined as follows:

$$\left[Y_{tN}^{(1)}\right] = [X_1]^{-1}[M_1]_N[X_2]^{-1} = \left[Z_{tN}^{(1)}\right]^{-1} \tag{26}$$

$$\left[Y_{tN}^{(2)}\right] = [X_1]^{-1}[M_2]_N[X_2]^{-1} = \left[Z_{tN}^{(2)}\right]^{-1} \tag{27}$$

The global impedance of transfer that takes into account the impacts of the discontinuities at the probe — MUT interface is given in the following equation,

$$Z_{tN}^T = Z_{tN}^{(2)} + Z_{tN}^{(1)} \tag{28}$$

As mentioned above in Equation (20), the new SUT effective permittivity is,

$$\varepsilon_{eff_N}^* = \frac{\left\{Z_{tN}^{(2)} + Z_{tN}^{(1)}\right\}^v}{\left\{Z_{tN}^{(2)} + Z_{tN}^{(1)}\right\}^m} \tag{29}$$

The dielectric complex relative permittivity is deducted from Equation (29) as follows,

$$\varepsilon_{r_N}^* = \frac{1}{D}\left\{\pi^2(h_2 + h_1) - \frac{h_2h_1 + \Delta h_{SUT}^2}{\Delta h_{SUT}}\right\}\varepsilon_{eff_N}^* \tag{30}$$

All dimensions' elements are identical, and the complex relative permittivity is expressed as given below:

$$\varepsilon_{r_N}^* = \varepsilon_{r_N}' - j\varepsilon_{r_N}'' \tag{31}$$

The dielectric constant is defined as ε_r', and the loss tangent is as shown in Equation (32)

$$\tan\delta_N = \frac{\varepsilon_{r_N}''}{\varepsilon_{r_N}'} \tag{32}$$

The transition from Equation (29) to Equation (30) is made by using a coefficient. In that case, the dielectric loss tangent, given in Equation (32), is the same for those deducted from effective and relative material intrinsic parameters. This conforms with reality, as the dielectric is not surrounded by metal.

3.3. Fitting Function

The test cell dimensions and its inhomogeneity as in Figure 1 cause resonances that appear when measurements are computed. These resonances significantly explain the structures' discontinuities. It means that despite the resolution of the interface impacts, these are not entirely sorted out as done in several techniques [22, 25]. In that case, an n-degree polynomial function has been set up as a model of discontinuity corrections. That is given as follows,

$$F = a_n X^n + a_{n-1} X^{n-1} + a_{n-2} X^{n-2} + a_{n-3} X^{n-3} + \dots a_0 \tag{33}$$

In the current situation, the procedure is chosen as 4-degree polynomial. The appropriate fitting function points are the same for all specimens. Also, the coefficients $a_n, \dots, a_0$ change according to the material to characterize.

4. RESULTS AND DISCUSSION

4.1. The Fabricated Test Cell

As illustrated in Figure 1(a), a test cell has been designed and fabricated to make possible the extraction of the dielectric constant and the loss tangent for thickness sized up to 3 mm. That fixture is plotted in Figure 3.

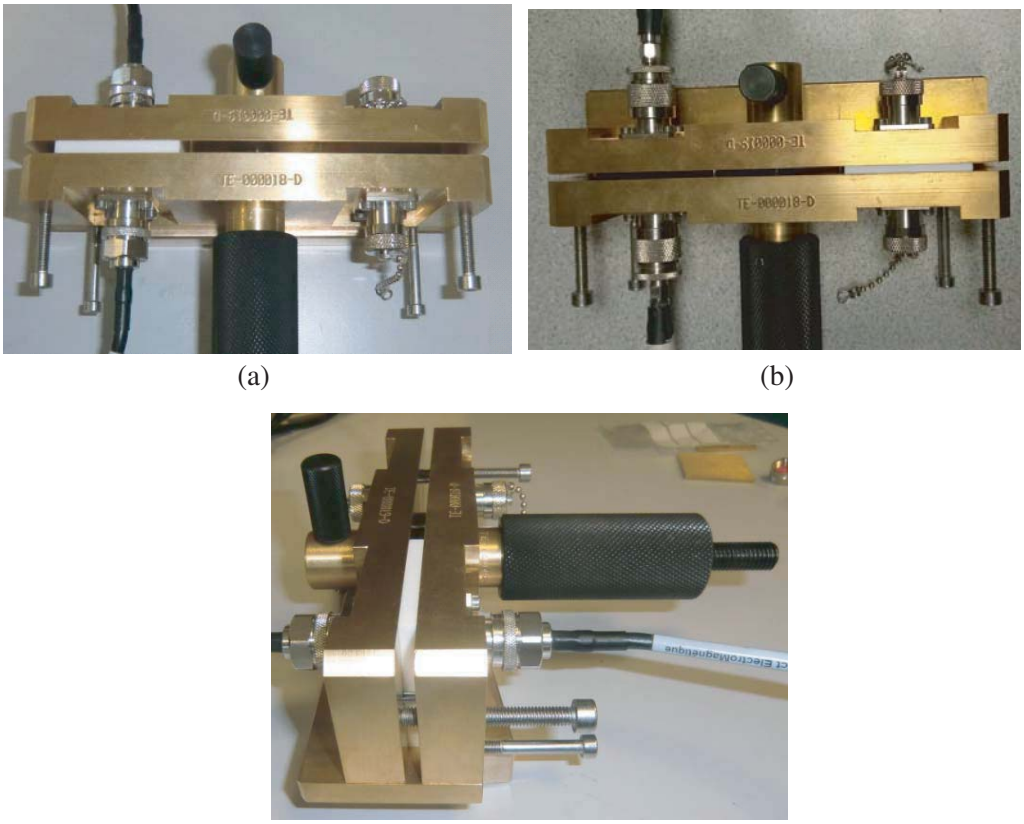

Figure 3. (a) Measurement of scattering parameters when the test cell is in the presence of the SUT. (b) Measurement of scattering parameters when the test cell is in the presence of the vacuum. (c) Side view of the test cell with the inserted SUT.

The test cell has a metallization under the SUT to improve the loss tangent data acquisition, as shown in Figure 3(c).

With that test cell (Figure 3), the possibility of measuring scattering parameters in the presence or not of the SUT is a reality. Both measurements can be simultaneously done. This way prevents us from wasting time. Besides, such a test cell, with the movable plate where the second plate is fixed and parallel, controls the SUT thickness for measurement in the vacuum presence.

4.2. Measurement Results and Discussion

The two approaches have been validated with Rogers RO4003C, FR-4 HTG-175, and Alumina 99.6%. Each material under test has two specimens with two discrete thicknesses. A vector network analyzer (VNA) Anritsu MS46522B is used before calculations. The previously developed equations are used on programming software. The test cell is manufactured with brass metal, and the main N-connectors have been used to facilitate the link between the VNA and the sample test cell. The relative permittivity ε'_r is the real part of the complex relative permittivity as defined in Equations (22) and (31). That parameter is shown in Figures 4, 6, and 8. We denote by "with discontinuities" the fact of using the impedance of discontinuity in the complex relative permittivity extraction process. On the other hand, when the discontinuity impedance is not used, we name it by "without discontinuities."

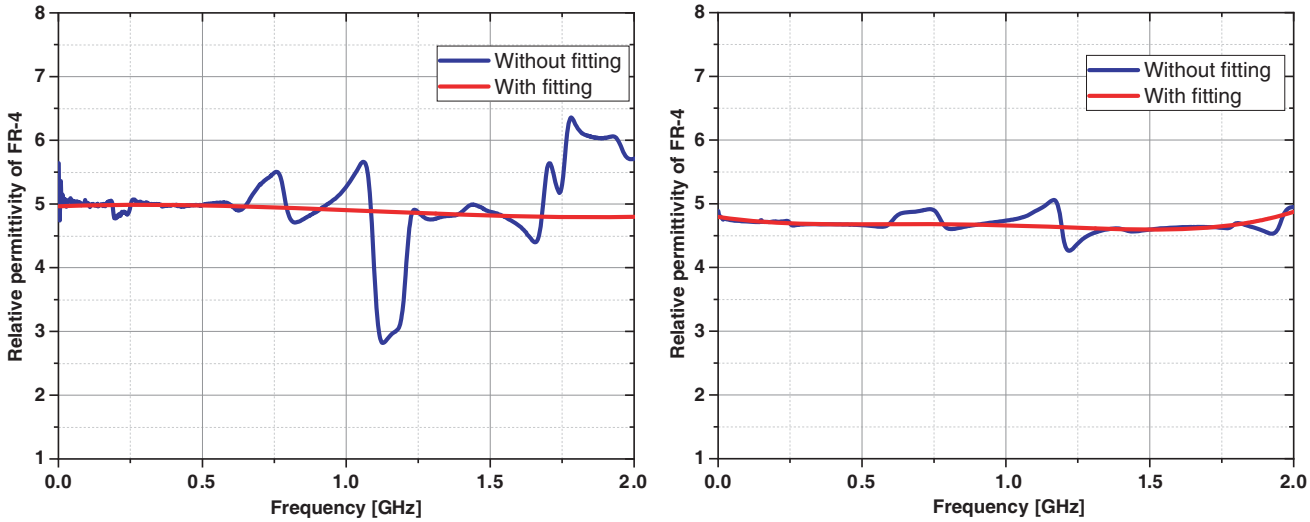

Figure 4. (a) FR-4 extracted without discontinuities. (b) FR-4 extracted with discontinuities.

At the contact interface probe — SUT, there are discontinuities impedances. In the extraction procedure previously developed through Equation (15), the discontinuity capacitance measurement is offered as illustrated in Equation (34)

$$C_d = \frac{Im\left(Y_d\right)}{\omega} \tag{34}$$

We can determine the specimen thickness gap by using Equation (18). As shown in Table 1, the SUT thicknesses are not the same for Alumina, FR-4, and RO4003C; even the two last materials have thicknesses slightly identical. All case-study (samples) are $5 \times 5\,\text{mm}^2$, but we have also used FR-4 in $5 \times 4\,\text{mm}^2$. The final results are the same. The inner conductor's outer diameter is $D = 5.2\,\text{mm}$, and Table 1 gives more details in SUT thicknesses.

The gap between two identical specimens depends on the SUT. That gap affects the measurement of the thickness when the SUT is not placed in the test cell. In the case of the FR4 that we used, that gap is equal to 0.734 mm, and in the case of Alumina, it becomes 2.067 mm. Figure 10 gives precious information about the SUT thickness's impact when the test cell is empty (in the absence of the SUT).

The discontinuity impedance depends on the sample under test as illustrated in Figure 11. We observe that all curves have 1.079 GHz as a resonance frequency. When the thickness is changed, this

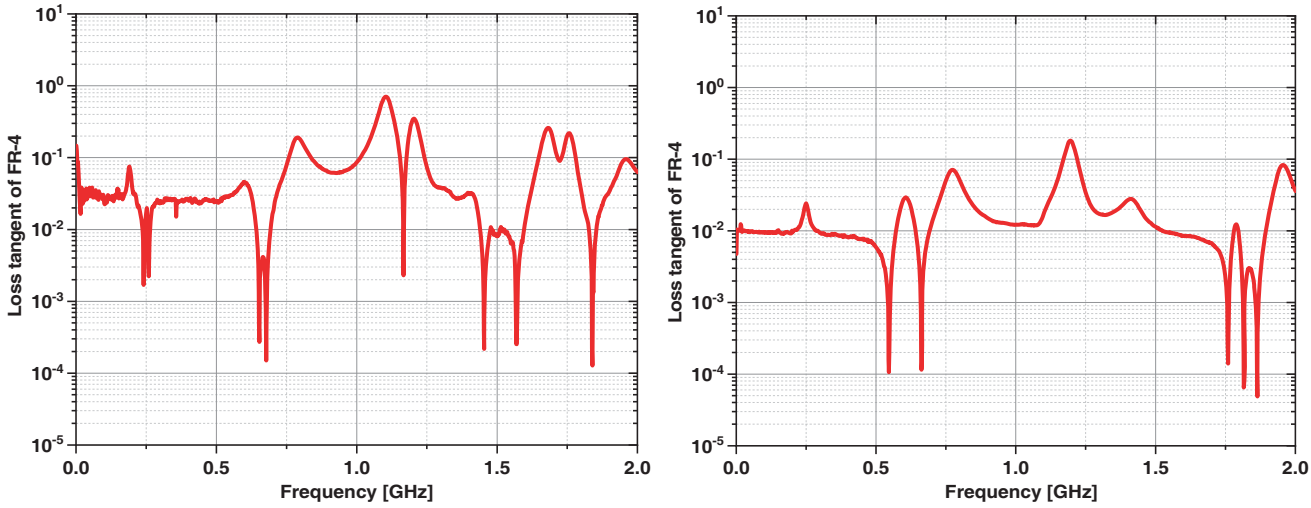

Figure 5. (a) FR-4 extracted without discontinuities. (b) FR-4 extracted with discontinuities.

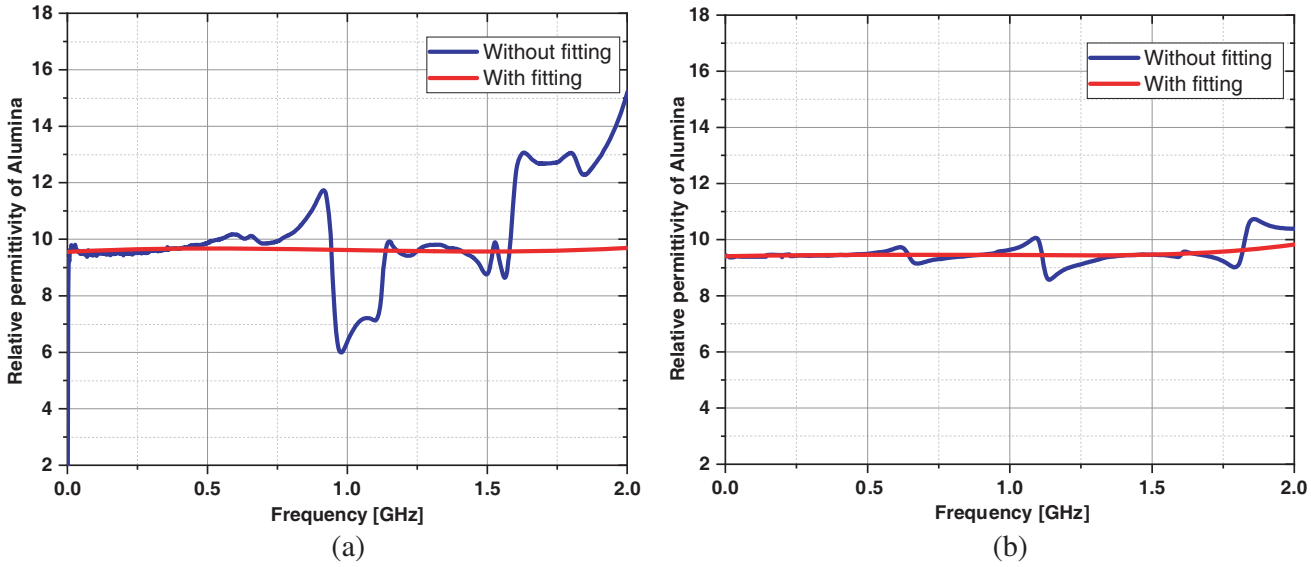

Figure 6. (a) Alumina 99.6% extracted without discontinuities. (b) Alumina 99.6% extracted with discontinuities.

Table 1. The Sample Under Test (SUT) thicknesses' values.

Thickness h (mm)	FR-4	Alumina 99.6%	Rogers RO 4003C
h_1	0.79	1.013	0.79
h_2	1.524	3.08	1.58
Δh	0.734	2.067	0.79

resonance frequency does not change. The three tested SUTs do not have the same dielectric constant, but the peaks are at the same frequency. It means that those peaks observed at 1.079 GHz are related to sample dimensions (length and width), neither to the material thickness nor to the complex permittivity. The specific dimensions that impact the discontinuity impedances are provided by the size (length and

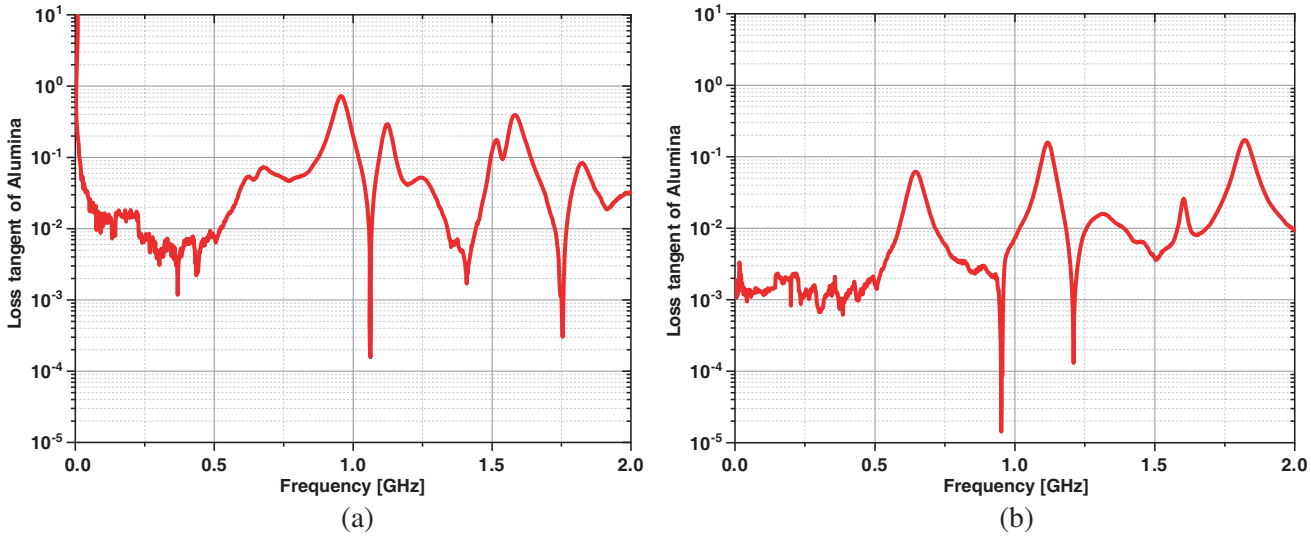

Figure 7. (a) Alumina 99.6% extracted without discontinuities. (b) Alumina 99.6% extracted with discontinuities.

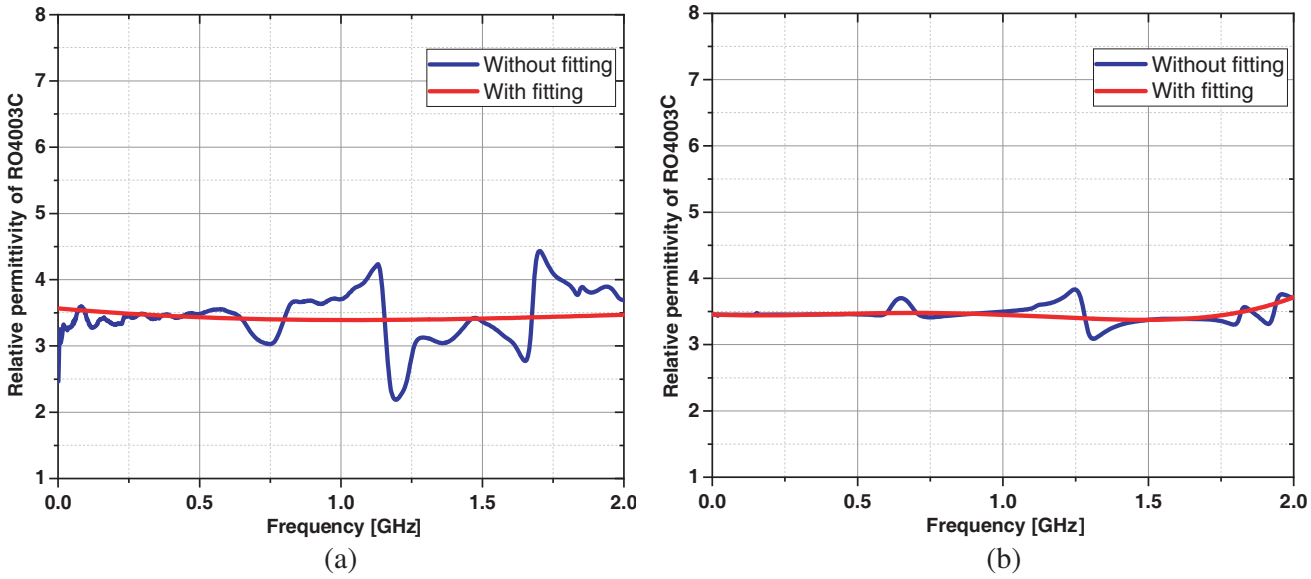

Figure 8. (a) RO4003C extracted without discontinuities. (b) RO4003C extracted with discontinuities.

width) of the SUT, not by the thickness. At the same time, the peak's level changes according to the SUT. This tells about the SUT effect in the extraction frequency range.

From the curves presented in Figure 10, the discontinuity depends on the SUT thickness, and the following Table 2 provides essential information on the contact interface repercussions.

It appears that the capacitance is proportional to the SUT thickness and works as a linear capacitor in this structure. As long as the thickness is significant, the discontinuity capacitor value does not change. We have also compared the polynomial function coefficients obtained when using different samples under test. Table 3 reflects the data comparison of the proper model function.

According to Equations (21) and (30), these coefficients do not depend on the frequency but the complex permittivity, effective parameter relative parameter, and thickness. From the behavior of the dielectric constant, the approach that uses discontinuity offers promising results. In addition, the loss

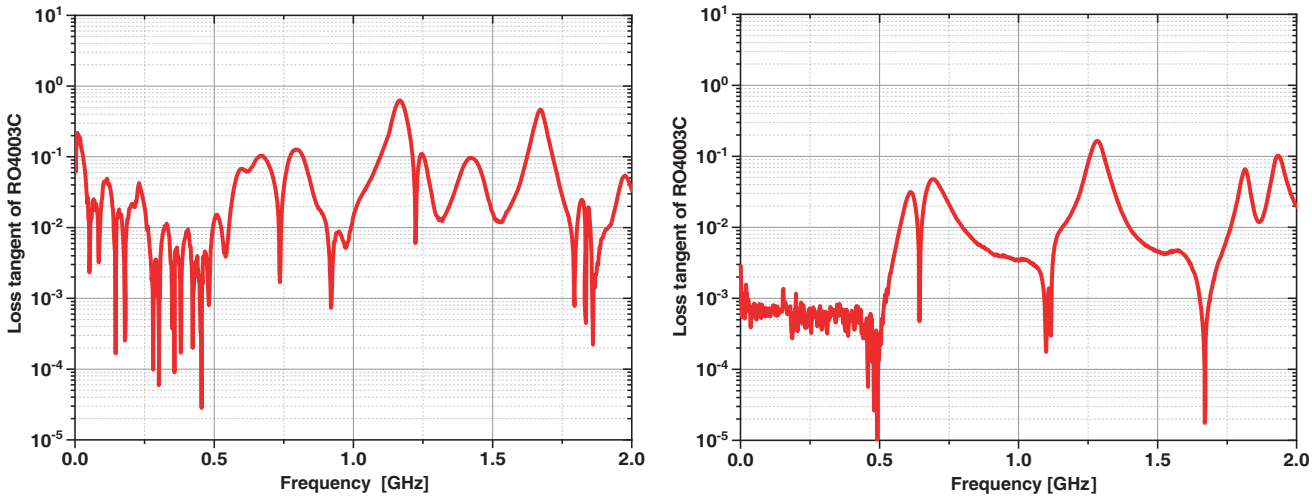

Figure 9. (a) RO4003C extracted without discontinuities. (b) RO4003C extracted with discontinuities.

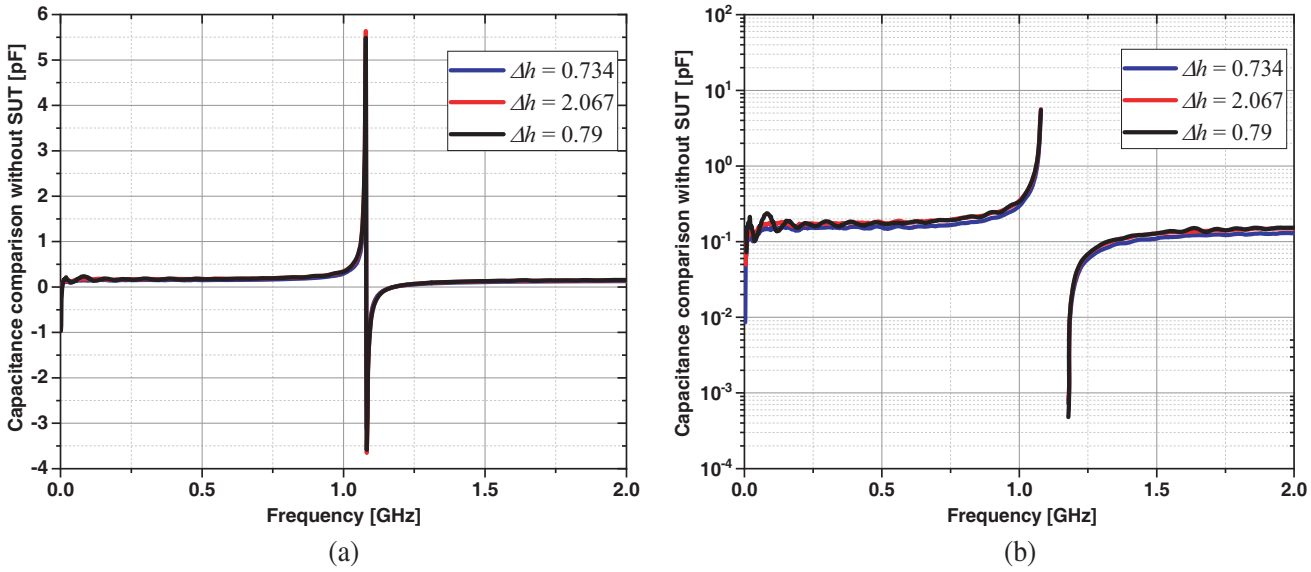

Figure 10. (a) The discontinuity capacitor for various sample thickness without the SUT. (b) Zoom of the discontinuity capacitor for various sample thickness without the SUT.

Table 2. Capacitance discontinuity value at the resonance frequency.

	FR-4		Rogers RO4003C		Alumina 99.6%	
	Vacuum	SUT	Vacuum	SUT	Vacuum	SUT
Capacitance C_d (pF)	4.894	7.495	5.489	8.928	5.637	15.801

tangent is well-adapted up to 550 MHz for all SUTs. The following Table 4 ensures indications in the SUT electric parameters.

The discontinuities approach is suitable for scanning frequency up to 2 GHz, while the second approach stops at 1.5 GHz. The same observation is made with the loss tangent. For the FR-4 HTG-

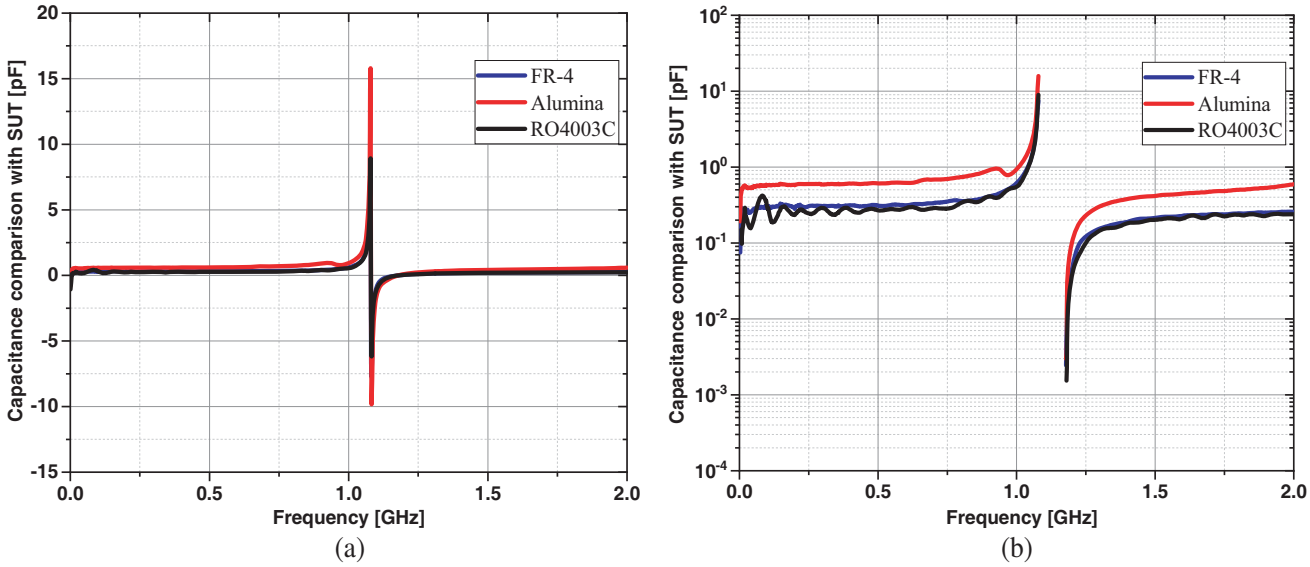

Figure 11. (a) The discontinuity capacitor for various sample thickness in the presence of the SUT. (b) Zoom of the discontinuity capacitor for various sample thickness in the presence of the SUT.

Table 3. The 4-degree polynomial function coefficient.

Polynomial coefficient	FR-4	Alumina 99.6%	Rogers RO 4003C
a_4	$0.09 - 0.013i$	$0.03 + 0.38i$	$0.084 + 0.09i$
a_3	$-0.32 + 0.068i$	$-0.066 - 1.072i$	$-0.264 - 0.243i$
a_2	$0.371 - 0.058i$	$0.02 + 0.875i$	$0.234 + 0.188i$
a_1	$-0.175 + 0.037i$	$0.025 - 0.207i$	$-0.055 - 0.043i$
a_0	$1.197 - 0.013i$	$1.832 - 7.506i * 10^{-4}$	$1.103 - 3.4065 * 10^{-4}$

Table 4. Electric parameter' (dielectric constant ε'_r and loss tangent $\tan\delta$) comparison of the SUT at 1 MHz.

	Without discontinuity		With discontinuity		Manufacturer	
	ε'_r	$\tan\delta$	ε'_r	$\tan\delta$	ε'_r	$\tan\delta$
FR-4	4.742	0.084	4.736	0.012	4.8	0.018
Alumina 99.6%	9.502	0.00729	9.42	0.00105	9.424	0.00031
Rogers RO4003C	3.542	0.024	3.548	$6 * 10^{-4}$	3.55	0.0021

175, the manufacturer finds $\varepsilon'_r = 4.8$ and $\tan\delta = 0.018$ at 1 MHz while these become $\varepsilon'_r = 4.2$ and $\tan\delta = 0.019$ at 1 GHz. As the manufacturer did not give information about the applied technique and its error evaluation to reach those results, we can notice a good accuracy between the two developed approaches in terms of the material relative permittivity. Due to the difference between loss tangent and relative permittivity obtained from both methods, some electromagnetic simulations (EMS) have been done through HFSS to study the suitability technique. The following curves plotted in Figure 12 help to well-understand the advantages and disadvantages of each model.

The approach using the discontinuities impedances at the probe and SUT contact interfaces is well adapted to extract complex relative permittivity of the SUT, according to Figure 12. On the other hand, this test cell is suitable for scanning the frequency range up to 5.5 GHz if we do not apply the

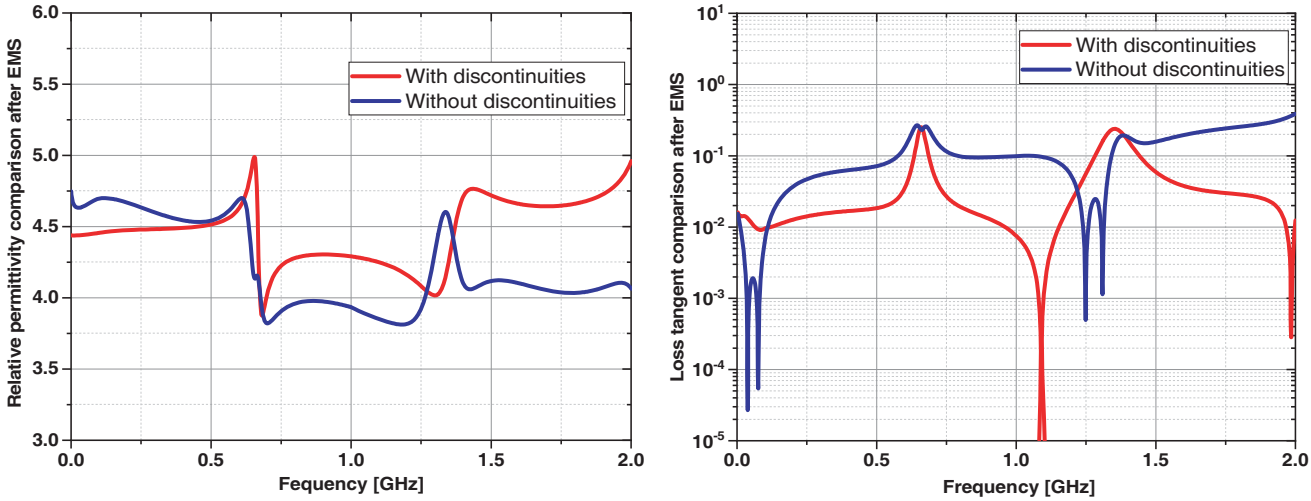

Figure 12. (a) Extracted relative permittivity after EMS when fixing $\varepsilon_r = 4.5$ in the entire frequency range. (b) Extracted loss tangent through EMS when fixing $\tan\delta_d = 0.02$ in the entire frequency range.

Table 5. Electric parameter' comparison of the SUT at 550 MHz.

	Without discontinuity			With discontinuity		
	ε'_r	$\tan\delta$	ε'_r :Fitting	ε'_r	$\tan\delta$	ε'_r: Fitting
FR-4	4.644	0.065	4.587	4.643	$9.501 * 10^{-4}$	4.679
Alumina 99.6%	10.01	0.016	9.672	9.561	$4.547 * 10^{-3}$	9.464
Rogers RO4003C	3.549	$7.644 * 10^{-3}$	3.426	3.449	$3.766 * 10^{-3}$	3.473

polynomial function for fitting results and covering the band of work up to 2 GHz. We observe that Figure 12 conforms with those drawn previously, Figures 4 to 9. Table 5 gives measured values of Alumina, FR4, and RO4003C at 550 MHz.

This table shows that electric parameters change with the frequency. Those parameters, especially the ones coming from the use of discontinuities, are close to the manufacturer.

5. CONCLUSION

Two probes in transmission have been presented through the development and experimental validation with three different materials in the frequency range 1 MHz–2 GHz. A test cell has been designed and a prototype manufactured. Various materials used to validate the processes cover a wide range of solid wafers (soft and hard wafers): FR-4 HTG-175, RO4003C, and Alumina 99.6%. Their thicknesses are between 0.79 mm and 3 mm. The SUT is located between both probes, and metal is placed under the characterized specimen to improve the loss tangent extraction (its accuracy). The SUT is a square whose dimensions are $5 \times 5\,\text{mm}^2$. Two approaches have been set up and the impact of discontinuities studied. Both techniques extract the interface parameter (discontinuity) and have been used to determine the real equivalent admittance (discontinuities are not included) or putting them in the global resolution (have them into). Both techniques approaches are well-adapted to the specimens to characterize through the designed test cell. A fitting possibility has been shown and developed through a mathematical model of an n-degree polynomial function. Its coefficients do not depend on the frequency, but the thickness and the SUT. Besides, the SUT dimensions prevent sweeping a vast range of frequencies. The fixture's dimensions and its design have to be improved to scan high frequencies with these techniques.

ACKNOWLEDGMENT

Grateful acknowledgment is made to Phéline Laboratory for great help during the validation process of the developed technique The authors also give thanks in a particular way to Pierre MOUKALA MPELE for the profusion pieces of advice and the reviewers for constructive criticisms that helped improve the paper.

REFERENCES

1. Lee, C.-K., J. McGhee, C. Tsipogiannis, S. Zhang, D. Cadman, A. Goulas, T. Whittaker, R. Gheisari, D. Engstrom, J. (Yiannis) Vardaxoglou, et al., "Evaluation of microwave characterization methods for additively manufactured materials," *Designs*, Vol. 3, 47, 2019.
2. Takach, A. A., F. M. Mbango, F. Ndagijimana, M. Al-Husseini, and J. Jomaah, "Two-line technique for dielectric material characterization with application in 3D-printing filament electrical parameters extraction," *Progress In Electromagnetics Research M*, Vol. 85, 195–207, 2019.
3. Lountala, M. G., F. M. Mbango, F. Ndagijimana, and D. Lilonga-Boyenga, "Movable short-circuit technique to extract the relative permittivity of materials from a coaxial cell," *Journal of Measurements in Engineering*, Vol. 7, 183–194, 2019.
4. Tiwari, N. K. and M. J. Akhtar, "Partially filled substrate integrated waveguide-based microwave technique for broadband dielectric characterization," *IEEE Transactions on Instrumentation and Measurement*, Vol. 68, 2907–2915, 2019.
5. Tosaka, T., K. Fujii, K. Fukunaga, and A. Kasamatsu, "Development of complex relative permittivity measurement system based on free-space in 220–330-GHz range," *IEEE Transactions on Terahertz Science and Technology*, Vol. 5, 102–109, 2015.
6. Severo, S. L. S., A. A. A. De Salles, B. Nervis, and B. K. Zanini, "Non-resonant permittivity measurement methods," *Journal of Microwaves, Optoelectronics and Electromagnetic Applications*, Vol. 16, 297–311, 2017.
7. Materials, L., J. Baker-jarvis, R. G. Geyer, J. H. Grosvenor, M. D. Janezic, C. A. Jones, B. Riddle, and C. M. Weil, "Dielectric characterization of low-loss materials," *IEEE Transactions on Dielectrics and Electrical Insulation*, Vol. 5, 571–577, 1998.
8. Moukanda Mbango, F., J. E. D. M'Pemba, F. Ndagijimana, and B. M'Passi-Mabiala, "Use of two open-terminated coaxial transmission-lines technique to extract the material relative intrinsic parameters," *IEEE Access*, Vol. 8, 138682–138689, 2020.
9. You, K. Y., "Effects of sample thickness for dielectric measurements using transmission phase-shift method," *International Journal of Advances in Microwave Technology (IJAMT)*, Vol. 1, 64–67, 2016.
10. Jebbor, N., S. Bri, and M. C. ElBoubakraoui, "Effective complex permittivity determination and microwave absorption properties of a granular dielectric composite material," *Procedia Computer Science*, Vol. 151, 1022–1027, 2019.
11. Costa, F., M. Borgese, M. Degiorgi, and A. Monorchio, "Electromagnetic characterisation of materials by using Transmission/Reflection (T/R) devices," *Electronics (Switzerland)*, Vol. 6, 2017.
12. Gonçalves, F. J. F., A. G. M. Pinto, R. C. Mesquita, E. J. Silva, and A. Brancaccio, "Free-space materials characterization by reflection and transmission measurements using frequency-by-frequency and multi-frequency algorithms," *Electronics*, Vol. 7, 3–6, 2018.
13. Bronckers, L. A. and A. B. Smolders, "Broadband material characterization method using a CPW with a novel calibration technique," *IEEE Antennas and Wireless Propagation Letters*, Vol. 15, 1763–1766, 2016.
14. Liao, X. and T. S. Wiedmann, "Characterization of pharmaceutical solids by scanning probe microscopy," *Journal of Pharmaceutical Sciences*, Vol. 93, 2250–2258, 2004.
15. Pometcu, L., A. Sharaiha, R. Benzerga, R. D. Tamas, and P. Pouliguen, "Method for material characterization in a non-anechoic environment," *Applied Physics Letters*, Vol. 108, 2–6, 2016.

16. Hyde, M. W., J. W. Stewart, M. J. Havrilla, W. P. Baker, E. J. Rothwell, and D. P. Nyquist, "Nondestructive electromagnetic material characterization using a dual waveguide probe: A full wave solution," *Radio Science*, Vol. 44, 1–13, 2009.
17. Antosiewicz, T. J., P. Wróbel, and T. Szoplik, "Magnetic probe for material characterization at optical frequencies," *Metamaterials VI*, Vol. 8070, 80700E, 2011.
18. Campos, D. C., J. C. A. Santos, and L. E. P. Borges, "Investigation of thermal effects in coaxial probe method and dielectric characterization of glycerol up to 140°C," *Journal of Microwaves, Optoelectronics and Electromagnetic Applications*, Vol. 18, 1–17, 2019.
19. Liu, W., H. Sun, and L. Xu, "A microwave method for dielectric characterization measurement of small liquids using a metamaterial-based sensor," *Sensors (Switzerland)*, Vol. 18, 18–27, 2018.
20. Bao, X., S. Liu, I. Ocket, J. Bao, D. Schreurs, S. Zhang, C. Cheng, K. Feng, and B. Nauwelaers, "A general line-line method for dielectric material characterization using conductors with the same cross-sectional geometry," *IEEE Microwave and Wireless Components Letters*, Vol. 28, 356–358, 2018.
21. López-Rodríguez, P., D. Escot-Bocanegra, D. Poyatos-Martínez, and F. Weinmann, "Comparison of metal-backed free-space and open-ended coaxial probe techniques for the dielectric characterization of aeronautical composites," *Sensors*, Vol. 16, 967–981, 2016.
22. Reynoso-Hernández, J. A., "Unified method for determining the complex propagation constant of reflecting and nonreflecting transmission lines," *IEEE Microwave and Wireless Components Letters*, Vol. 13, 351–353, 2003.
23. Lin, X. and B. C. Seet, "Dielectric characterization at millimeter waves with hybrid microstrip-line method," *IEEE Transactions on Instrumentation and Measurement*, Vol. 66, 3100–3102, 2017.
24. Ouslimani, H. H., R. Abdeddaim, and A. Priou, "Free-space electromagnetic characterization of materials for microwave and radar applications," *PIERS Proceedings*, 128–132, Hangzhou, China, 2005.
25. Moukanda Mbango, F. and F. Ndagijimana, "Electric parameter extractions using a broadband technique from coaxial line discontinuities," *International Journal of Scientific Research and Management*, Vol. 7, 248–253, 2019.